Long-period spectral features of the Sumatra-Andaman 2004 earthquake rupture process

E. Clévédé, B. Bukchin, P. Favreau, A. Mostinskiy, † A Aoudia, G. F Panza

Geophysical Journal International

Geophys. J. Int. (2012) **191,** 1215–1225 doi: 10.1111/j.1365-246X.2012.05482.x

Long-period spectral features of the Sumatra–Andaman 2004 earthquake rupture process

E. Clévédé,[1] B. Bukchin,[2] P. Favreau,[1,*] A. Mostinskiy,[2,†] A. Aoudia[3] and G. F. Panza[3,4]

[1] *Institut de Phyisque du Globe de Paris, UMR* 7154, *Paris, France. E-mail: clevede@ipgp.fr*
[2] *Institute of Earthquake Prediction Theory and Mathematical Geophysics Russian Academy of Sciences, Moscow, Russian Federation*
[3] *The Abdus Salam International Center for Theoretical Physics, Trieste, Italy*
[4] *Department of Geosciences, University of Trieste, Italy*

Accepted 2012 March 27. Received 2012 March 27; in original form 2009 March 25

SUMMARY

The goal of this study is to investigate the spatial variability of the seismic radiation spectral content of the Sumatra–Andaman 2004 earthquake. We determine the integral estimates of source geometry, duration and rupture propagation given by the stress glut moments of total degree 2 of different source models. These models are constructed from a single or a joint use of different observations including seismology, geodesy, altimetry and tide gauge data. The comparative analysis shows coherency among the different models and no strong contradictions are found between the integral estimates of geodetic and altimetric models, and those retrieved from very long period seismic records (up to 2000–3000 s). The comparison between these results and the integral estimates derived from observed surface wave spectra in period band from 500 to 650 s suggests that the northern part of the fault (to the north of 8°N near Nicobar Islands) did not radiate long period seismic waves, that is, period shorter than 650 s at least. This conclusion is consistent with the existing composite short and long rise time tsunami model: with short rise time of slip in the southern part of the fault and very long rise time of slip at the northern part. This complex space-time slip evolution can be reproduced by a simple dynamic model of the rupture assuming a crude phenomenological mechanical behaviour of the rupture interface at the fault scales combining an effective slip-controlled exponential weakening effect, related to possible friction and damage breakdown processes of the fault zone, and an effective linear viscous strengthening effect, related to possible interface lubrication processes. While the rupture front speed remains unperturbed with initial short slip duration, a slow creep wave propagates behind the rupture front in the case of viscous effects accounting for the long slip duration and the radiation characteristics in the northern segment.

Key words: Earthquake dynamics; Earthquake source observations; Surface waves and free oscillations; Theoretical seismology.

1 INTRODUCTION

The 2004 December 26, Sumatra–Andaman earthquake is not only the largest event that has occurred globally since 1964, but also the first of such a size which has been studied using a wide spectrum of observations with characteristic periods ranging from a fraction of seconds to months (e.g. see Bilek *et al.* 2007). The detailed space-time description of the rupture process given by the different authors makes a straightforward comparison of the different proposed models difficult. On the other side, integral characteristics of an earthquake's rupture, as shown by McGuire *et al.* (2001) and Clévédé *et al.* (2004), estimated by the second order moments of the slip rate distribution over the fault related to the source size, orientation, duration and rupture velocity vector, can be useful for a robust comparison of models obtained from different observations and their combinations.

In the case of the Sumatra–Andaman earthquake, the size of the source is constrained by both HF *P*-wave energy radiation (e.g. Lomax 2005; Ishii *et al.* 2005; Ni *et al.* 2005; Kanamori 2006; Gusev *et al.* 2007), *T* waves (e.g. DeGroot-Hedlin 2005), and very long-period data (normal modes, tsunami) (e.g. Ammon *et al.* 2005; Lay *et al.* 2005; Park *et al.* 2005; Piatanesi & Lorito 2007; Fujii & Satake 2007). The earthquake ruptured a 1300 km long section of the Sunda and Sumatra trenches with up to 20 m of slip (Banerjee *et al.* 2007; Chlieh *et al.* 2007). Despite its extreme complexity in the rupture process, several groups of investigators recognized three large scale segments along strike; namely Sumatra segment to the South, Nicobar and Andaman to the North.

Results of some of these studies suggest that there is a spatial variability of the seismic radiation spectral content, the slip

*Deceased 2010 May 14
†Deceased 2009 June 30

distribution varying along the strike with both a long tail and a probable slow component to the North.

Moreover, this segmentation is consistent with the variations of the physical properties along the rupture area found by Kennett & Cummins (2005), Shapiro *et al.* (2008), and Lorito *et al.* (2010).

In this paper, we try to investigate this spatial variation. The second moments (see the appendix for main definitions) of the coseismic slip distribution are compared for models constructed from seismological, geodetic, altimetric and tide gauge measurements. As a constraint in the comparison we use the estimates of the same integral moments retrieved from observed surface wave spectra in the period band from 500 to 650 s (Bukchin & Mostinskiy 2007). Then the models are compared through their integral characteristics and their compatibility is discussed. Finally, the possibility to reproduce the main features of the rupture process considering a simple dynamic source model is investigated.

2 INTEGRAL ESTIMATES FROM SURFACE WAVE SPECTRA ANALYSIS

To estimate the best double couple, duration and geometry of the source we have used amplitude spectra of the second and third orbits of fundamental Love and Rayleigh modes in the spectral range from 500 to 650 s. The records were processed by the frequency-time and polarization analysis package FTAN (Levshin *et al.* 1989).

We selected 24 Love wave records and 22 Rayleigh wave records from IRIS and GEOSCOPE stations. For the computation of the synthetic spectra of surface waves displacement a model is considered, for the Earth structure, with weak lateral Inhomogeneity (Woodhouse 1974; Babich *et al.* 1976). In the source region and under the receivers, the 3SMAC model (Ricard *et al.* 1996) is used for the crust and the PREM model for the mantle and for the quality factor used for attenuation correction. The results of surface wave amplitude spectra inversion are summarized in Table 1.

The moment tensor describing the source in the instantaneous point source approximation is obtained by the joint inversion of surface wave amplitude spectra and first arrival polarities at worldwide distributed stations (Lasserre *et al.* 2001). The solution gives a focal mechanism described by the following values of strike, dip and slip: 330°, 8°, 105°, respectively. The estimate of the source depth is about 13 km. The estimated value of seismic moment is 0.52×10^{23} N m.

To estimate the 2nd moments of moment tensor density (stress glut) the nodal plane dipping to the northeast is considered as the fault plane. The source depth (13 km) and focal mechanism are fixed at the values obtained in instantaneous point source approximation. Usually when double–couple parameters are obtained from periods long enough to consider the source as an instant in time and a point in space, the seismic moment value should be fixed as well. But in this case the periods are not sufficiently long, therefore the seismic moment is recomputed when determining the source second-order moments. The duration, the geometry of the source and the instant centroid velocity are estimated from the same amplitude spectra of fundamental Love and Rayleigh modes in the same spectral band (from 500 to 650 s) that was used for the inversion in instantaneous point source approximation. The final estimate of the seismic moment is equal to 0.84×10^{23} N m.

The 2nd moments of moment tensor density can be expressed in by formulas (A8)–(A14) in terms of six parameters: Δt—integral estimate of source duration, $l_{\max}$—integral estimate of maximal mean size of the source, ϕ_l—the angle between the strike axis and source major axis, $l_{\min}$—integral estimate of minimal mean size of the source, v—integral estimate of the absolute value of instant centroid mean velocity **v** and ϕ_v—the angle between the strike axis and the vector **v**. We consider as estimates of these parameters the optimal values that minimize the misfit between observed and synthetic surface wave amplitude spectra. We search them by a systematic exploration of the 6-D parameter space. To characterize the degree of resolution of every of these source characteristics we calculate partial residual functions. The inversion yields an integral estimate of duration being of about 160 s, a characteristic source length (major axis length) of 300–400 km, while the minor axis length is poorly resolved between 0 and 200 km. The average instant centroid velocity estimate is about 2 km s^{-1}. The angles giving the orientation of the major axis and of the velocity vector orientations are measured clockwise on the foot wall starting from the strike axis. They are consistent with each other and the correspondent residual functions attain their minimum values at 15°. The residual functions for the integral estimates of source parameters characterizing their resolution are given in Fig. 1.

The propagation of the rupture may be characterized by the directivity ratio d proposed by McGuire *et al.* (2001). This parameter is defined as the ratio of the average velocity of the instant centroid over the apparent rupture velocity which is equal to $l_{\max}/\Delta t$ (see appendix). For a unilateral rupture where the slip on a rectangular fault nucleates at one end and propagates to the other end at a uniform rupture velocity with a uniform slip distribution, $d = 1$. For a symmetric bilateral rupture that initiates in the centre and propagates to both end of a fault with uniform rupture velocity and with uniform slip distribution, $d = 0$. Predominantly bilateral ruptures correspond to $0 \leq d \leq 0.5$ while predominantly unilateral ruptures correspond to $0.5 \leq d \leq 1$. The value about 0.8 to 0.9 obtained in this analysis reveals a unilateral (northward) rupture propagation.

3 COMPARISON OF DIFFERENT MODELS

3.1 Models used in this study

Among the numerous studies of the Sumatra–Andaman earthquake source rupture process, nine are selected where different type of data either by inversion or as constraints are considered.

Lay *et al.* (2005) performed the seismological analysis and the tsunami modelling using altimetric and tide gauge data. Ammon *et al.* (2005) used very broadband seismological data from 80 to 3000 s, to retrieve the slip distribution model used in this study (hereinafter referred as model II), and from 5 to 2000 s (hereinafter referred as model III) and the 1-D model (IRT 1-D model) based on data from 80 to 500 s used to address the estimation of the source

Table 1. Integral moments of the coseismic slip distribution retrieved from observed surface wave spectra in the period band from 500 s to 650 s

Strike (°)	Dip (°)	Rake (°)	Seismic moment (N.m)	Source depth (km)	Integral duration (s)	Length of major axis (km)	Strike axis major axis (°)	Length of minor axis (km)	Instant centroid velocity (km s^{-1})	Strike axis – velocity angle (°)
330	8	105	0.8410^{23}	13	160	300 − 400	15	0 − 200	2	15

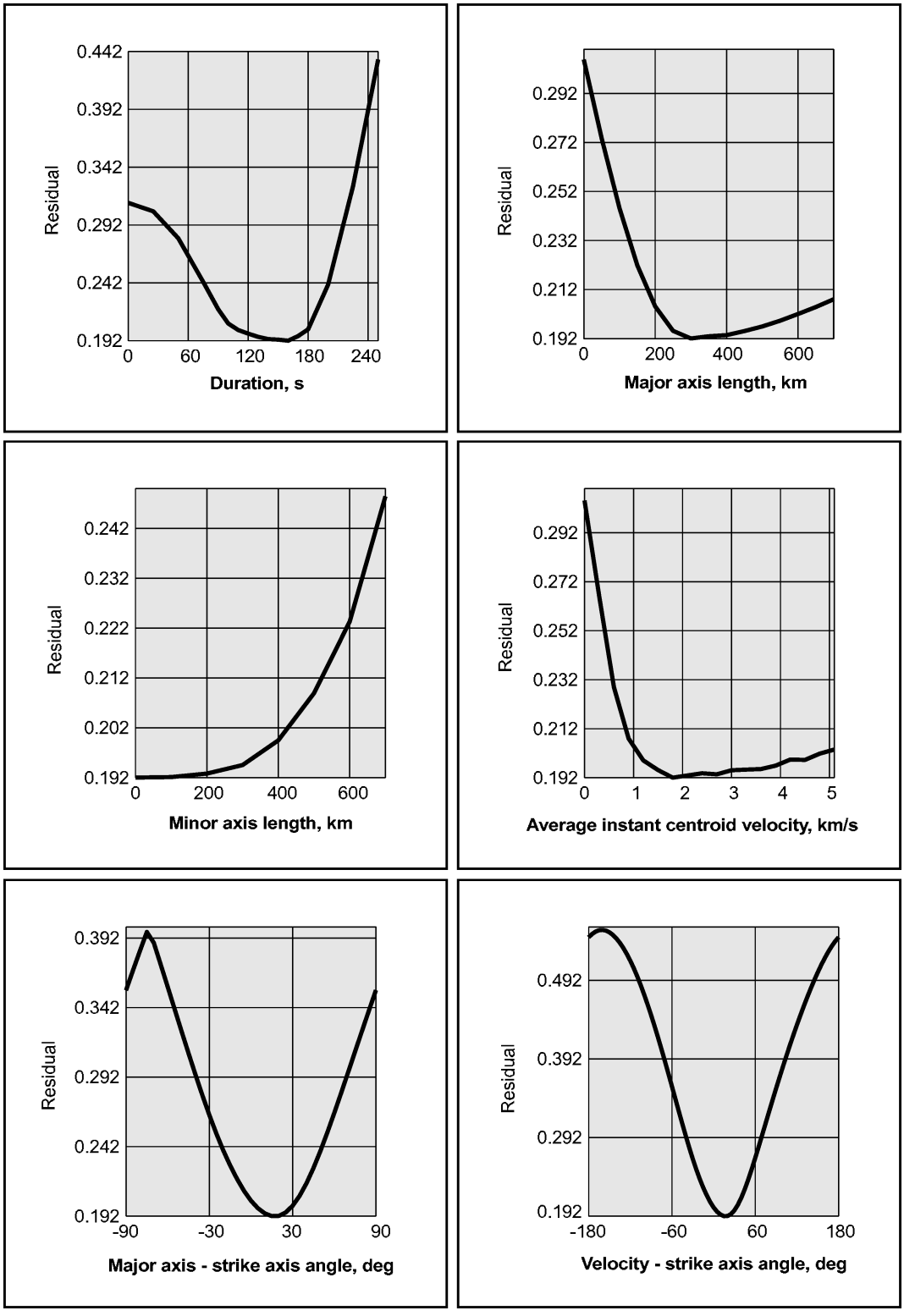

Figure 1. Residual functions for the source integral characteristics given by the stress glut moments of total degree 2 obtained from surface wave analysis.

duration. Models from Banerjee *et al.* (2007) and Pietrzak *et al.* (2007) use far-field and near field geodetic data (GPS). For Pietrzak *et al.* (2007) we consider the model obtained by joint inversion of these two sets of data. Rhie *et al.* (2007) performed a joint inversion of geodetic and long-period (100–500 s) seismological data. Piatanesi & Lorito (2007) used tide gauge waveform to retrieve the rupture process of the tsunami source. Fujii & Satake (2007) performed a joint inversion of tide gauge and altimetric data. Sladen & Hébert (2008) inverted for the source of the tsunami using altimetric data. Lorito *et al.* (2010) combined tide gauges, satellite altimetry and far-filed GPS recordings in a joint inversion to infer simultaneously the kinematic parameters of the rupture and the rigidity of

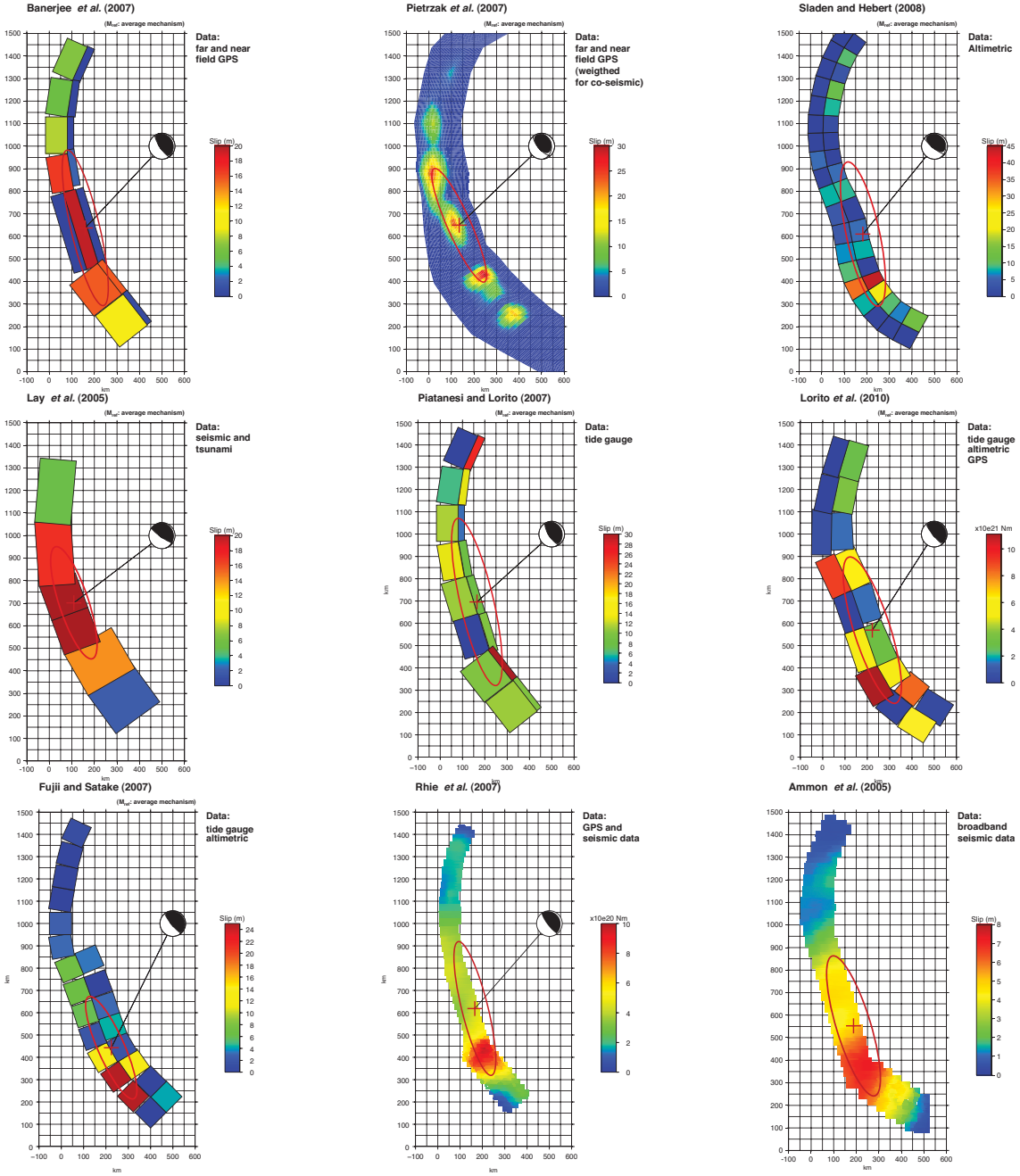

Figure 2. Set of slip distribution models used in this study. Beach balls are showing average focal mechanisms.

the source zone, we consider here their best model. Fault geometry, slip distribution and average mechanism for these models are represented on Fig. 2.

Except for the model II of Ammon *et al.* (2005), the source model parametrization and the slip distribution given by these studies are used. In the case of Ammon *et al.* (2005), the model II is digitized from their fig. S6, available with the supporting on-line materials for horizontal displacement only, therefore the average mechanism for this model is not shown.

3.2 Integral estimates of models

To compare these models and our results of long period surface wave inversion, the integral characteristics of these models corresponding to the stress glut rate moments of degree 0, 1 and 2 directly from their theoretical definitions (see appendix) are computed.

3.2.1 *Spatial characteristics*

For the nine models the spatial centroid location and the ellipse characteristics (principal axes length and orientation) are considered. In the case of Lay *et al.* (2005) the model includes two separate types of slip: the first one corresponds to a rise time of 50 s, and the second one corresponds to a rise time of 3500 s. The two corresponding 'sub-models' are considered, as well, and there integral estimates are summarized in Table 2 and illustrated in Figs 2 and 3.

The spatial integral characteristics of all the complete models are fairly compatible. The length of the minor axis ranges from 116 to

Table 2. Spatial integral characteristics of the models.

Model	Azimuth of major axis (°)	Length of minor axis (km)	Length of major axis (km)	Length of major axis for truncated model (km)	Seismic moments ratio for truncated and complete models
Banerjee *et al.* (2007)	347	127	708	361	0.67
Sladen & Hébert (2008)	348	147	654	359	0.84
Pietrzak *et al.* (2007)	336	104	550	402	0.70
Piatanesi & Lorito (2007)	347	150	768	411	0.60
Lorito *et al.* (2010)	342	162	688	417	0.68
Fujii & Satake (2007)	336	119	500	390	0.90
Rhie *et al.* (2007)	346	117	617	341	0.74
Ammon *et al.* (2005)	343	152	648	403	0.79
Lay *et al.* (2005) total slip	342	131	523	327	0.66
Lay *et al.* (2005) fast slip	328	116	327	–	–

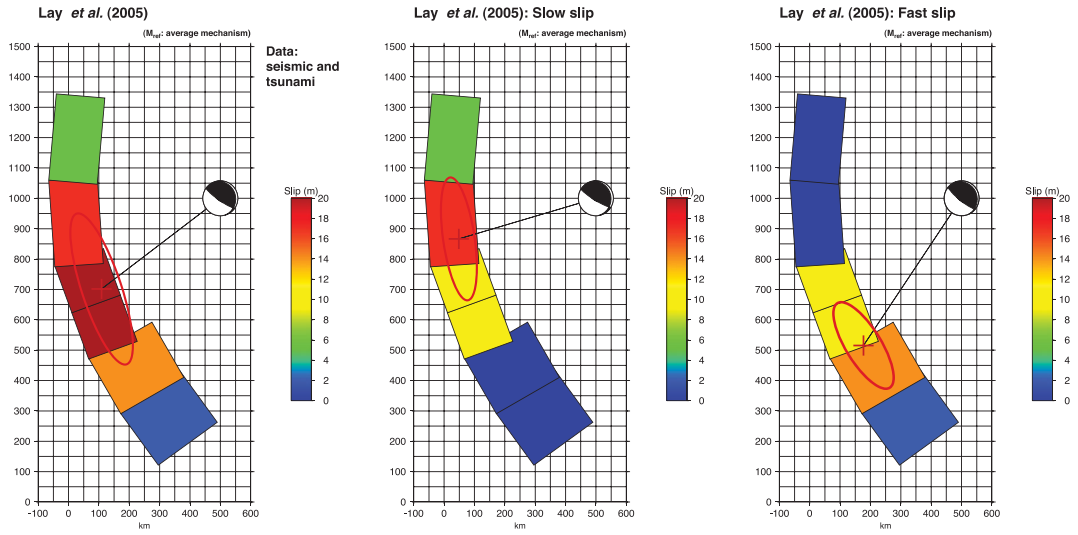

Figure 3. Total, slow and fast slip distribution for the Lay *et al.* (2005) model.

152 km, the length of the major axis ranges from 523 to 768 km, but the estimates of the length of the major axis are not compatible with our estimate obtained from surface wave inversion (from 300 to 400 km). On the other side, the estimate for the 'fast slip submodel' proposed by Lay *et al.* (2005) (327 km), which does not require 'fast slip' to the North of Nicobar segment (about 8°N), fits quite well our estimate based upon surface-wave inversion.

The result of the comparison of the lengths of the major axis for all models truncated by excluding slip to the North of 8° are shown in Table 2 and Fig. 4. For Banerjee *et al.* (2007) and Piatanesi & Lorito (2007) (using similar fault models) this truncation corresponds to the removal of the eight northernmost segments of the model, while for the other more detailed models, this corresponds to the removal of the part of the fault North of 8°. In this case, the estimates of Lay *et al.* (2005) (327 km), Banerjee *et al.* (2007) (361 km), Rhie *et al.* (2007) (341 km), Fujii & Satake (2007) (390 km) and Sladen & Hébert (2008) (359 km) fit our estimate, while for Ammon *et al.* (2005) (403 km), Pietrzak *et al.* (2007) (402 km), Piatanesi & Lorito (2007) (411 km) and Lorito *et al.* (2010) (417 km) the estimates correspond to the upper boundary of our estimate.

Table 2 also shows the seismic moments ratio for truncated and complete models. The seismic moment of the truncated models is from 60 to 90 per cent of the moment of the complete models.

The scalar moment M_0 is not considered here since the rigidity μ used in the different models is not the same and this difference in the assumed value of μ impacts on the absolute values of slip. Therefore the comparison is made considering normalized values of the slip distribution on the fault for each model. This choice does not affect our conclusions since the integral estimates of the source size depends only on the relative distribution of slip.

3.2.2 Integral estimate of duration

The moment rate dependence on time is given by Ammon *et al.* (2005) for three different models: The IRT 1-D model is obtained by inverse Radon transform using Rayleigh waves for periods from 80 to 500 s; the two other models use very long-period seismic waves, respectively 100 to 3000 s for model II, and 250 to 2000 s for model III. We also consider the moment rate obtained by (Ishii *et al.* 2005) using *P*-waves radiated in the period range 1 to 5 s.

The computed integral estimate of the earthquake source duration for these four models is reported in Table 3. While the estimates pertinent to the models obtained inverting high frequency *P* waves or very long periods Rayleigh waves are much larger (293 s, 241 s and 247 s, respectively) than our surface waves estimate (160 s), the estimate obtained for the IRT 1-D model using long period waves (187 s) is close to our estimate.

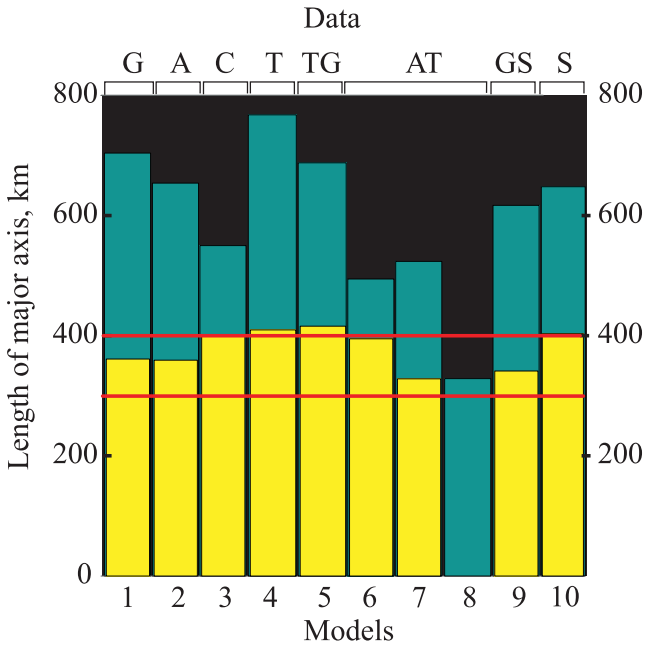

Figure 4. Estimates of the major axis length for the different models. Green columns correspond to complete models, yellow columns correspond to models truncated to the north of 8°N. Red lines show our lower and upper estimates from surface wave inversion in the period band 500–650 s. G - GPS data, A - altimeters data, C - GPS, altimeters and tide gauges data, T - tide gauges data, AT - altimeters and tide gauges data, GS - GPS and seismological data, S - very broad band (from 100 s to 3000 s) seismological data. Model 1 - model C by Banerjee *et al.* (2007); model 2 - Sladen & Hébert (2008); model 3 - model asv8 by Pietrzak *et al.* (2007): all available data are used, but near field GPS data weighted in order to obtain only coseismic slip; model 4 - Piatanesi & Lorito (2007); model 5 - Lorito *et al.* (2010); model 6 - Fujii & Satake (2007); model 7 - Lay *et al.* (2005) (total slip); model 8 - Lay *et al.* (2005) (fast slip); model 9 - Rhie *et al.* (2007); model 10 - Ammon *et al.* (2005).

Table 3. Temporal integral characteristics of the models.

Model	Period band	Integral duration
Ishii *et al.*	1-5 s	293 s
IRT 1D	80-500 s	187 s
Model II	100-3000 s	241 s
Model III	250-2000 s	247 s

3.2.3 Comparison of models

The existing models can be separated in two families:

(i) Geodetic and/or altimetric models and/or tide gauge data and/or seismological models retrieved from very long period seismic records (up to 2000–3000 s): Ammon *et al.* (2005) models II and III, Lay *et al.* (2005), Banerjee *et al.* (2007), Pietrzak *et al.* (2007), Rhie *et al.* (2007), Piatanesi & Lorito (2007), Fujii & Satake (2007), Sladen & Hébert (2008), Lorito *et al.* (2010).

(ii) Seismological models obtained inverting long period records, but shorter than about 700 s: Lay *et al.* (2005) short rise time model, Ammon *et al.* (2005) 1-D IRT model, and this study.

The preferred explanation of the difference between the main characteristics of these two families is the coseismic slip on the northernmost part (North of 8°) with rise time large enough to be not detectable in the long-period radiation, but still within the seismic band and tsunamigenic. The comparison between the different major axis lengths reported on Fig. 4 shows coherency among the different models accordingly with the type of data set used either jointly or singularly. For instance the GPS and both altimeters and tide gauges data when used jointly provide a reasonable average of when they are used singularly. This does apply to GPS and seismological data. Therefore this is likely a relative measure of robustness of the already published models. Furthermore the agreement between the truncated long models to the North with our long period estimates do confirm the existence of two classes of slip during the Sumatra–Andaman earthquake.

4 MODELLING OF COMBINED SHORT AND LONG SLIP DURATIONS

We associate short and long slip duration with short and long rise time, respectively. The unusual rise times observed along the Andaman fault segment suggest a broad-band rupture dynamics. Understanding the non-linear coupling between these different rupture timescales has important implication in terms of earthquake energy release and of frictional dissipation, at the fault scales unraveled by seismic observation of limited frequency bandwidth. This is investigated by a dynamic modelling of the rupture and its spectral characterization, for example, moment distribution, energy release and radiation efficiency.

4.1 Dynamic modelling

Earthquake dynamics is classically simulated using a 3-D finite difference as a frictional shear rupture process embedded in an infinite homogeneous elastic medium. A simplified planar surface geometry is assumed here for the three segments, and the rupture is assumed to propagate with a constant rake along these segments. At the fault scale, local shear traction on the rupture plane is estimated using phenomenological interface laws such as slip-weakening (Ida 1972; Andrews 1976; Ohnaka *et al.* 1987) or rate-and-state-dependent laws (Dietrich 1979; Ruina 1980). The actual unresolved gap between seismic and laboratory experiment scales inevitably implies compromises on at least one of the aspect of the physics of the source.

Classical linear slip-weakening friction law, extensively used in seismology to study dynamic rupture, is the simplest criterion that account for a finite fracture energy without stress and slip rate discontinuities. This criterion involves a characteristic length, or slip-weakening distance, and shear is a fixed function of slip, which sets the amount of energy lost to fracture and frictional dissipation. Standard slip-dependent friction law can not explain the long rise times observed in part of the rupture. Standard rate-and-state friction law, introduced to capture some experimental observations of both steady velocity dependence, transient slip and time dependence of friction, is defined in terms of slip rate and a single state variable for which slip or aging phenomenological evolution laws are introduced to include a memory of previous slip episodes. At seismic slip rate scales, this kind of friction laws leads to a problematic logarithmic slip rate dependence (Di Toro *et al.* 2004; Rice 2006) and behaves mostly like slip weakening and velocity dependent friction laws.

In the following, we adopt on the basis of its simplicity, the effective interface law proposed by Nielsen *et al.* (2000) and Nielsen & Carlson (2000)

$$\tau = \theta + \eta\delta\dot{u} \qquad \text{if } \delta\dot{u} > 0 \tag{1}$$

$$\tau < \theta \qquad \text{if } \delta\dot{u} = 0, \tag{2}$$

where

$$\dot{\theta} = \alpha \left[V_c(\tau_s - \theta(t)) - \delta\dot{u}(t)(\theta(t) - \tau_d) \right], \qquad \theta(0) = \tau_s \tag{3}$$

τ is the shear stress parallel to the rake, $\delta\dot{u}$ the slip rate, θ the state of the system, η a frictional viscosity, $1/\alpha$ a characteristic slip weakening length, V_c a characteristic healing velocity, τ_s the initial strength, τ_d the viscosity-free dynamic strength. In this simple model, the absolute level of shear pre-stress τ_0 does not interfere with the dynamics and only the strength excess $\tau_e = \tau_s - \tau_0$ and the dynamic stress drop $\Delta\tau_d = \tau_0 - \tau_d$ are relevant in the model. This effective interface law depends, as the rate-and-state friction laws, on the slip history and the instantaneous slip rate. This law is derived from the rate-and-state law originally proposed by Carlson & Batista (1996) for lubricated interfaces. It also bares similarities with the piecewise continuous friction law considered by Cochard & Madariaga (1994).

Assuming the characteristic healing timescale to be large compared to the rupture slip timescale, the first term in the right hand side of the state evolution (eq. 3) can be neglected. Under this hypothesis, the interface law can be restated as non-linear slip weakening law including a frictional viscous term.

$$\tau = \tau_s - (\tau_s - \tau_d)\left(1 - e^{(-\alpha\delta u)}\right) + \eta\delta\dot{u}, \qquad \text{if } \delta\dot{u} > 0, \tag{4}$$

where δu is the slip. The form of this frictional law retains for simplicity two competing effects: a slip-controlled exponential weakening, related to the effective interface breakdown due to progressive friction and damage processes of the fault zone, and a viscous frictional effect, related to an effective interface lubrication. During most of the seismic rupture, this provides a very good approximation of the dynamics (Carlson & Batista 1996) up to the arrest phase where healing effects become important. In the under-damped regime ($\eta = 0$), slip time is controlled by the inertial time, while in the over-damped regime slip time increases and slip rates decay more gradually as a result of the increased dissipation associated with the mobilization of effective interface lubrication processes. Another response is that produced by very rapid changes in slip velocity. In the event where the interface is subjected to an instantaneous jump in velocity, the model predicts an instantaneous change of shear strength controlled by the effective frictional viscous response ($\|\tau\| = \eta\|\delta\dot{u}\|$). The rupture front speed is mainly controlled by the dynamic stress drop and the slip weakening rate, while slip duration is controlled by the frictional viscosity.

Two rupture models have been built up that fit some of the average rupture characteristics observed by many authors: (i) the rupture propagated from South to North on three segments: Sumatra, Nicobar and Adaman; (ii) The dynamics of the rupture is heterogeneous among these segments and the seismic efficiency seems to decrease as the rupture propagates toward North; (iii) the seismic efficiency depends on the rupture speed and the sliding velocity, which depend on the geometry, the local strength excess and the frictional properties. Kanamori (2006) proposed estimated kinematic and energetic parameters segment by segment that will be used here to constrain the mechanical rupture modelling.

We consider a planar rupture surface geometry with three main segments with width (km) × length (km) of 180 × 420, 130 × 325 and 120 × 570 for the Sumatra, Nicobar and Andaman segments, respectively. This geometry is similar to the one of Lay *et al.* (2005), used also by Kanamori (2006). Rupture is limited to these segments by prescribing outside of them a lower pre-stress state. The rupture mode is mostly mode III and accordingly the largest expected rupture velocity is the *S*-wave velocity of the crust. The strength excess τ_e is far less important for mode-III rupture than for mode-II, and will set to zero here. Variations of the fracture energy is prescribed by varying $1/\alpha$ only, and the mechanical parameters of the two models are summarized in Table 4 segment by segment. We consider two models: a under-damped model with $\eta = 0$ in all the three segments, and a damped model where viscous effects are mainly concentrated in the Andaman segment.

Table 4. Parameters for the dynamic models, averaged segment by segment.

	$\overline{\Delta\tau_d}$ (MPa)	D_c (m)	ν (MPa s/m)
Model without fault viscosity:			
Sumatra	3.11	10	0
Nicobar	7.43	28	0
Andaman	2.07	10	0
Model with fault viscosity:			
Sumatra	3.11	10	0
Nicobar	6.06	19	1
Andaman	2.89	10	20

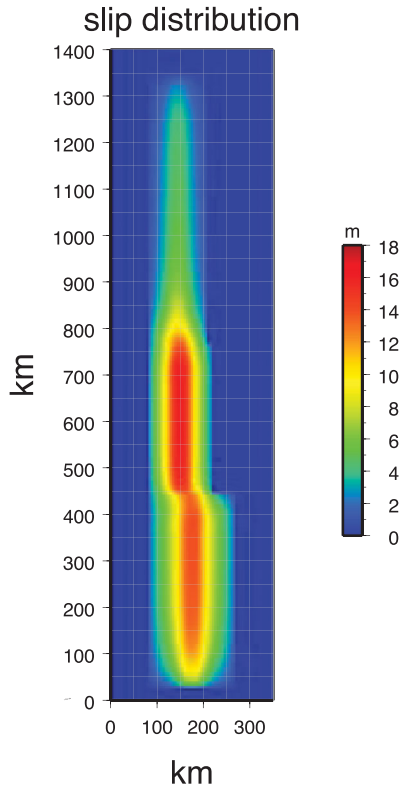

Figure 5. Final slip distribution for the dynamical source models.

Both models exhibit very similar characteristics beside a long rise-time in the Andaman segment for the damped model. The final slip of these models is shown in Fig. 5. In Table 5 the average characteristics (moment and seismic efficiency) of the models are summarized. For the seismic efficiency of a regularized rupture without stress singularity the following definition is used

$$\eta_R = \frac{E_R}{W_{\text{elast}}} \tag{5}$$

$$W_{\text{elast}} = \int_{\text{Fault}} \frac{1}{2}(\tau_0 - \tau_1)(\delta u_1 - \delta u_0)\mathrm{d}S_{\text{Fault}} \tag{6}$$

Table 5. Normalized seismic moments and radiation efficiency obtained by: — Kanamori (2006) — using classical slip-dependent friction (no viscosity) — velocity strengthening (with viscosity)

		Kanamori (2006)	no viscosity	with viscosity
Total M_0		1	1	1
Sumatra	M_0	0.46	0.48	0.46
	η_R	0.21	0.25	0.28
Nicobar	M_0	0.34	0.33	0.34
	η_R	0.053	0.07	0.05
Andaman	M_0	0.20	0.20	0.20
	η_R	–	−0.20	−0.24

$$E_R = W_{\text{elast}} + \int_{\text{Fault}} \int_0^1 (\delta u - \delta u_0) \mathrm{d}\tau \mathrm{d}S_{\text{Fault}}, \tag{7}$$

where subscripts 0 and 1 correspond to initial and final states, respectively. W_{elast} is the potential energy change, E_R is the radiated seismic energy, and η_R is the radiation efficiency. For a uniform distribution of the stress drop ($\tau_0 - \tau_1$), this definition matches the one of Rice (1980) and the well known definition $\eta_R = 2\mu/(\overline{\tau_0 - \tau_1})E_R/M_0$, where $M_0 = \mu(\overline{\delta u_1 - \delta u_0})S_{\text{Fault}}$ is the seismic moment and μ the shear modulus. It is important to note that the seismic energy E_R is a theoretically invariant and global number that can be evaluated in different way in far field or on the fault, as fault surface integrals (Rivera & Kanamori 2005), but any partitioning of the fault in time and/or space (like segment partitioning) gives different results. Local negative values of E_R, as defined by (7), are common at the places where the rupture looses mechanical energy as it propagates.

To analyse the space-time fault dynamics evolution in the case of the damped model, contour maps of the sliding velocity is shown in Fig. 6 for this model. On the Sumatra and the Nicobar segments, where viscosity is null and small, respectively, the rise time is of the order of 50 s at the nucleation and decreases as the rupture propagates toward North at almost the shear wave speed (3 km s^{-1}, for this model). In contrast in the Adaman segment, where a stronger viscosity is prescribed, while the rupture front still propagates at almost the shear wave speed ($\simeq$3 km s^{-1}) associated with a rapid pre-slip, a large creep wave is observed following the rupture front. This creep wave is travelling now at a group velocity of about 1 km s^{-1} with a slip creep velocity of about 1 cm s^{-1}. For large times, that is, long after the rupture front has reached the end of the Andaman segment and the creep wave has diffused, a residual uniform flow creep at 1 mm s^{-1} can still be observed with an exponential decay in time. Such a cross over regime is a result of the competing effects between the exponential slip weakening and the linear viscous frictional strengthening. While the speed of the rupture front remains the same as in the under-damped case, viscosity effects control a diffusive creep wave propagation at much lower speed than the *S*-wave speed. An effect reminiscent of wave propagation in elasto-viscoplastic media.

The main spectral characteristics of the earthquake source, together with the observed complex space-time sliding process, can be quite well reproduced when using a simple form of the phenomenological interface law that retains only an exponential slip weakening and a linear frictional viscous strengthening of the interface. This provides interesting insight on the competitive effects between slip weakening effects, related to effective interface frictional and damage breakdown processes, and strengthening effects, related to effective interface lubrication viscous frictional processes, for extended source rupture dynamics of great earthquakes that break multiple segments in relation to potential along strike variation of the subduction interface.

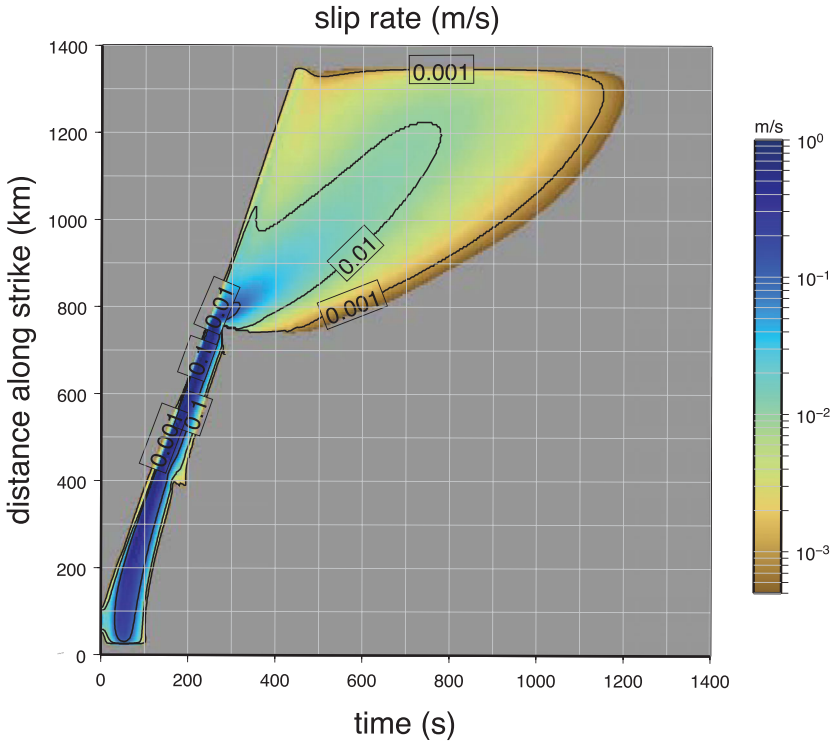

Figure 6. Slip rate distribution in time at the 'ridge line' of the final slip distribution (the line of maximum slip for a given position along the strike) for the dynamic model with fault viscosity.

4.2 Spectral features

Even with its crude parametrization, the model is able to mimic the main features of the Sumatra–Andaman rupture process in terms of moment distribution, energy release and radiation efficiency as determined by Lay *et al.* (2005), Ammon *et al.* (2005) and Kanamori (2006).

To analyse the source time function of our model, the amplitude spectra of the moment rate function integrated over two parts of the fault in the bandwidth 0–2.5 mHz (periods longer than 400 s) are computed. The first part of the fault includes the southern segments, which corresponds to the short slip duration submodel of Lay *et al.* (2005) and to the spatial truncation used in Section 3.2.1. The second part corresponds to the segments of Lay *et al.* (2005) model with long slip duration, that is, the northern segment here; in our model fast and slow slip velocities are not separated. The normalized amplitude spectra of the moment rate and ratio of these spectra are shown in Fig. 7.

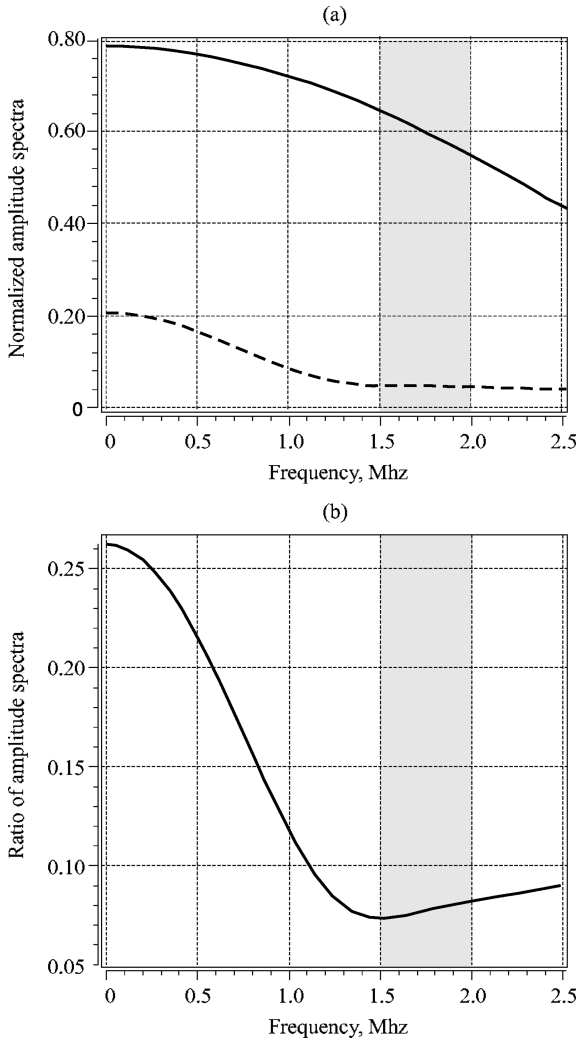

Figure 7. (a) Comparison of the amplitude spectra of the moment rate function integrated over two parts of the fault: 'southern' part segments (solid line) and 'northern' part (dashed line). Both spectra are normalized by the maximum value of the amplitude spectra of the moment rate integrated over the entire fault. (b) The ratio of amplitude spectra integrated over the northern segment to amplitude spectra integrated over the southern segment. The grey areas represent the spectral band used for the surface wave integral estimates.

The southern part and the northern part account for 80 per cent and 20 per cent of the total moment, respectively (Table 5 and Fig. 7a). Due to the large diffusive contribution on the northern part, the ratio of the relative contribution of each part to the moment rate spectra is decreasing with frequency (Fig. 7b). For periods below 800 s (frequencies above 1.25 mHz), this ratio becomes too small to be reliably detected by seismic data in this spectral domain in the northern part of the rupture.

5 CONCLUSION

In this paper, we try to investigate the spatial variation of the seismic radiation spectral content of the Sumatra–Andaman 2004 earthquake. Results of other authors confirm this variability.

Considering Long period Rayleigh wave directivity, Ammon *et al.* (2005) stated that the modelling of a simple propagating rupture suggests that Rayleigh waves observations at periods shorter than 600 s are compatible with a north-northwest propagation of a rupture at a speed of about 2.5–3 km s^{-1} for 400–600 km from the southern end of the fault. Both observations for short periods, from a few seconds down to a tenths of seconds, and periods longer than 600 s are only partly accounted for by this model and suggest that additional slip extended in either time, space, or both is required to explain the observed very long period surface wave data.

Considering seismic and tsunami observations, Lay *et al.* (2005) suggest a composite slip model with short slip duration (50 s rise time) in the southern portion of the rupture, and long slip duration (3500 s rise time) to the North of the Nicobar segment (about 8°N). Such a long rise time cannot generate seismic waves, however the radiation of very long period seismic energy in the Northern part of the fault is required by seismic observations (Ammon *et al.* 2005; Park *et al.* 2005), which suggests a rise time of slow slip, very large but inside the seismic period band. The existence of such a slow slip with rise time of 1000–2000 s is confirmed by tsunami data analysis (Song *et al.* 2005; Hirata *et al.* 2006; Singh *et al.* 2006; Seno & Hirata 2007). Furthermore the latitudinal heterogeneous distribution of the early after-slip along the Sumatra-Andaman structure (Chlieh *et al.* 2007) with a sharp decrease in amplitude within the slow-slip section corroborates the combination of two different rupture behavior. In fact the coseismic slow-slip part of the Sumatra-Andaman rupture has likely sustained the missing rate-strengthening observed after-slip.

In this study we show the that integral estimates of the source length and duration for the models obtained from geodetic and/or very long period seismic or altimetric data are larger than our estimates based on long period surface wave inversion (Tables 2 and 3, and Fig. 4).

Integral estimates of the size for the same models truncated to the North of 8°N fit our long period surface wave estimate (Tables 2, and Fig. 4). Integral estimate of duration for the IRT 1-D model (Ammon *et al.* 2005) using long period Rayleigh waves fit our long period surface wave estimate (Table 3).

Summarizing these results, and relying on the fact that the size of the source is constrained by HF P-wave energy radiation (Lomax 2005; Ishii *et al.* 2005; Ni *et al.* 2005; Kanamori 2006; Gusev *et al.* 2007), HF T-waves (DeGroot-Hedlin 2005), and very long-period data (normal modes, tsunami) (Ammon *et al.* 2005; Lay *et al.* 2005; Park *et al.* 2005; Fujii & Satake 2007; Piatanesi & Lorito 2007), we propose that the Northern part of the Sumatra-Andaman fault (to the North of 8°) radiated very long period seismic energy and did

not radiate long period seismic energy at periods shorter than 650 s. We show that simple dynamic modeling can reproduce this feature as long as effective viscous faulting effects are introduced.

It is important to note that we do not present this very simple model as an actual description of the Sumatra-Andaman source process. For example, Park *et al.* (2007) demonstrate that some low order normal modes exhibit unmodelled peculiar amplitude behavior, showing that a more complex rupture history at large scale should be investigated.

ACKNOWLEDGMENTS

The authors are very grateful to Jean-Pierre Vilotte for his help in the finalisation of this work. Comments and suggestions by Associated Editor Massimo Cocco and anonymous reviewer during the review process have greatly improved this manuscript. This research was done while B.B. and A.M. were visiting the Institut de Physique du Globe de Paris, thanks to a grant from MESR in France. B.B. is also supported by the Basic Research Program N4 of the Presidium of Russian Academy of Sciences. Some figures have been produced with the Generic Mapping Tools software (Wessel & Smith 1998). This is IPGP (UMR CNRS 7154) contribution number 3341.

REFERENCES

Ammon, C.J. *et al.*, 2005. Rupture process of the 2004 Sumatra-Andaman earthquake, *Science,* **308,** 1133–1139.

Andrews, D.J., 1976. Rupture velocity of plane strain shear crack, *J. geophys. Res.,* **81,** 5679–5687.

Backus, G.E., 1977a. Interpreting the seismic glut moment of total degree 2 or less, *Geophys. J. R. astr. Soc.,* **51,** 1–25.

Backus, G.E., 1977b. Seismic source with observable glut moment of spatial degree two, *Geophys. J. R. astr. Soc.,* **51,** 27–45.

Babich, V.M., Chikachev, B.A. & Yanovskaya, T.B., 1976. *Surface Waves in a Vertically Inhomogeneous Elastic Half-space with Weak Horizontal Inhomogeneity,* Izv. Akad. Nauk SSSR, Fizika Zemli 4, pp. 24–31.

Banerjee, P., Pollitz, F., Nagarajan, B. & Bürgmann, R., 2007. Coseismic slip distributions of the 26 December 2004 Sumatra-Andaman and 28 March 2005 Nias earthquakes from GPS static offsets, *Bull. seism. Soc. Am.,* **97,** S86–S102.

Bilek, S.L., Satake, K. & Sieh, K., 2007. Introduction to the special issue on the 2004 Sumatra-Andaman earthquake and the Indian ocean tsunami, *Bull. seism. Soc. Am.,* **97,** S1–S5.

Bukchin, B. & Mostinskiy, S., 2007. Integral source characteristics of the Sumatra earthquakes of December 26, 2004 and March 28, 2005, *Journal of Volcanology and Seismology,* **1**(4), 263–273.

Carlson, J.M. & Batista, A.A., 1996. Constitutive relation for the friction between lubricated surfaces, *Phys. Rev. E,* **53**(4), 4153–4165.

Clévédé, E., Bouin, M.-P., Bukchin, B., Mostinskiy, A. & Patau, G., 2004. New constraints on the rupture process of the 17 August 1999 Izmit earthquake deduced from estimates of stress glut rate moments, *Geophys. J. Int.,* **159,** 931–942.

Chlieh, M. *et al.*, 2007. Coseismic slip and afterslip of the great M_w 9.15 Sumatra-Andaman earthquake of 2004, *Bull. seism. Soc. Am.,* **97,** S152–S173.

Cochard, A. & Madariaga, R., 1994. Dynamic faulting under rate-dependent friction, *Pure appl. Geophys.,* **142,** 419–445.

DeGroot-Hedlin, C.D., 2005. Estimation of the rupture length and velocity of the Great Sumatra earthquake of Dec 26, 2004 using hydroacoustic signals, *Geophys. Res. Let.,* **32,** L11303, doi:10.1029/2005GL022695.

Dietrich, J.H., 1979. Modeling of rock friction 1. Experimental results and constitutive equations, *J. geophys. Res.,* **84**(5), 2161–2168.

Di Toro, G., Goldsby, D.L. & Tullis, T.E., 2004. Friction falls towards zero in quartz rock as slip velocity approaches seismic rates, *Nature,* **427,** 436–439.

Fujii, Y. & Satake, K., 2007. Tsunami source of the 2004 Sumatra-Andaman earthquake inferred from tide gauge and satellite data, *Bull. seism. Soc. Am.,* **97,** S192-S207.

Gusev, A., Guseva, E.M. & Panza, G.F., 2007. Size and duration of the high-frequency radiator in the source of the 2004 December 26 Sumatra earthquake, *Geophys. J. Int.,* **170,** 1119–1128.

Hirata, K., Satake, K., Tanioka, Y., Kuragano, T., Hasegawa, Y., Hayahsi, Y. & Hamada, N., 2006. The 2004 Indian Ocean tsunami: tsunami source model from satellite altimetry, *Earth Planets Space,* **58,** 195–201.

Ida, Y., 1972. Cohesive force across the tip of a longitudinal-shear crack and Griffith's specific surface energy, *J. geophys. Res.,* **77**(20), 3796–3805.

Ishii, M., Shearer, P.M., Houston, H. & Vidale, J.E., 2005. Extent, duration and speed of the 2004 Sumatra-Andaman earthquake imaged by the Hi-Net array. *Nature,* **435**(7044), 933–936, doi:10.1038/nature03675.

Kanamori, H., 2006. The radiated energy of the Sumatra-Andaman earthquake, *Earthquake Radiated Energy and the Physics of Faulting,* Geophys. Monogr. Ser. 170, American Geophysical Union, Washington DC.

Kennett, B.L.N. & Cummins, P.R., 2005. The relationship of the seismic source and subduction zone structure for the 2004 December 26 Sumatra-Andaman earthquake, *Earth planet. Sci. Lett.,* **239,** 1–8.

Lasserre, C., Bukchin, B., Bernard, P., Tapponnier, P., Gaudemer, Y., Mostinskiy, A. & Dailu, R., 2001. Sources parameters and tectonic origin of the 1996 June 1 Tianzhu ($M_w = 5.2$) and 1995 July 21 Yongden ($M_w = 5.6$) earthquakes near the Haiyuan fault (Gansu, China), *Geophys. J. Int.,* **144**(1), 206–220.

Lay, T. *et al.*, 2005. The great Sumatra-Andaman earthquake of 26 December 2004, *Science,* **308,** 1127–1133.

Levshin, A.L., Yanovskaya, T.B., Lander, A.V., Bukchin, B.G., Barmin, M.P., Ratnikova, L.I. & Its, E.N., 1989. *Seismic Surface Waves in Laterally Inhomogeneous Earth,* ed., Keilis-Borok, V.I., Kluwer, Dordrecht.

Lomax, A., 2005. Rapid estimation of rupture extent for large earthquakes: application to the 2004, M9 Sumatra-Andaman mega-thrust, *Geophys. Res. Lett.,* **32,** L10314, doi:10.1029/2005GL022437.

Lorito, S., Piatanesi, A., Cannelli, V., Romano, F. & Melini, D., 2010. Kinematics and source zone properties of the 2004 Sumatra-Andaman earthquake and tsunami: Nonlinear joint inversion of tide gauge, satellite altimetry, and GPS data, *J. geophys. Res.,* **115,** doi:10.1029/2008JB005974.

McGuire, J.J., Zhao, L. & Jordan, T.H., 2001. Teleseismic inversion for the second-degree moments of earthquake space-time distributions, *Geophys. J. Int.,* **145**(3), 661–678.

Ni, H., Helmberger, D. & Kanamori, H., 2005. Energy radiation from the Sumatra earthquake, *Nature,* **434,** 582.

Nielsen, S.B., Carlson, J.M. & Olsen, K.B., 2000. Influence of friction and fault geometry on earthquake rupture, *J. geophys. Res.,* **105**(3), 6069–6088.

Nielsen, S.B. & Carlson, J.M., 2000. Rupture pulse characterization: self-healing, self-similar, expanding solutions in a continuum model of fault dynamics, *Bull. seism. Soc. Am.,* **90,** 1480–1497.

Ohnaka, M., Kuwara, Y. & Yamamoto, K., 1987. Constitutive relations between dynamic physical parameters near a tip of the propagating slip zone during stick slip shear failure, *Tectonophysics,* **144,** 109–125.

Park, J. *et al.*, 2005. Earth's Free Oscillations Excited by the 26 December 2004 Sumatra-Andaman Earthquake, *Science,* **308,** 1139–1144.

Park, J., Amoruso, A., Crescentini, L. & Boschi, E., 2007. Long-period toroidal Earth free oscillations from the great Sumatra-Andaman earthquake observed by paired laser extensometers in Gran Sasso, Italy, *Geophys. J. Int.,* **173,** 887–905.

Piatanesi, A. & Lorito, S., 2007. Rupture process of the 2004 Sumatra-Andaman earthquake from tsunami waveform inversion, *Bull. seism. Soc. Am.,* **97,** S223–S231.

Pietrzak, J. *et al.*, 2007. Defining the source region of the Indian Ocean Tsunami from GPS, altimeters, tide gauges and tsunami models, *Earth planet. Sci. Lett.,* **261,** 49–64.

Rhie, J., Dreger, D., Bürgmann, R. & Romanowicz, B., 2007. Slip of the 2004 Sumatra-Andaman earthquake from joint inversion of long period global seismic waveforms and GPS static offsets, *Bull. seism. Soc. Am.,* **97,** S115–S127.

Rice, J.R., 1980. The mechanics of earthquake rupture, in *Physics of the Earth's Interior,* pp. 555–649, ed. Boschi, A.M.D a. E., North-Holland, Amsterdam.
Rice, J.R., 2006. Heating and weakening of faults during earthquake slip, *J. geophys. Res.,* **11,** B05311, doi:10.1029/2005JB004006.
Rivera, L. & Kanamori, H., 2005. Representations of the radiated energy in earthquakes. *Geophys. J. Int.,* **162,** 148–155, doi:10.1111/j.1365-246X.2005.02648.x.
Ricard, Y., Nataf, H.-C. & Montagner, J-P., 1996. The 3SMAC model. Confrontation with seismic data, *J. geophys. Res.,* **101,** 8457–8472.
Ruina, A.L., 1980. Friction laws and instabilities: a quasistatic analysis of some dry frictional behavior, *PhD thesis*, Brown University, Providence, RI.
Seno, T. & Hirata, K., 2007. Did the 2004 Sumatra-Andaman Earthquake Involve a Component of Tsunami Earthquakes?, *Bull. seism. Soc. Am.,* **97,** S296–S306.
Shapiro, N.M., Ritzwoller, M.H. & Engdahl, E.R., 2008. Structural context of the Great Sumatra-Andaman Islands earthquake, *Geophys. Res. Lett.,* **35**, L05301, doi:10.1029/2008GL033381.
Singh, S.K., Ortiz, M., Gupta, H.K. & Ramadass, D.G.A., 2006. Slow slip below Port Blair, Andaman, during the great Sumatra-Andaman earthquake of 26 December 2004, *Geophys. Res. Lett.,* **33,** L03313, doi:10.1029/2005GL025025.
Sladen, A. & Hébert, H., 2008. On the use of satellite altimetry to infer the earthquake rupture characteristics: application to the 2004 Sumatra event, *Geophys. J. Int.,* **172,** 707–714.
Song, Y.T., Ji, C., Fu, L.-L., Zlotnicki, V., Shum, C.K. & Yi, Y., 2005. The 26 December 2004 tsunami source estimated from satellite radar altimetry and seismic waves, *Geophys. Res. Lett.,* **32,** L20601, doi: 10.1029/2005GL023683.
Wessel, P. & Smith, W.H.F., 1998. New improved version of the Generic Mapping Tools released, *EOS, Trans. Am. geophys. Un.,* **79,** 579, doi:10.1029/98EO00426.
Woodhouse, J.H., 1974. Surface Waves in the Laterally Varying Structure, *Geophys. J. R. astr. Soc.,* **90,** 713–728.

APPENDIX A: SECOND MOMENTS APPROXIMATION. CHARACTERISTICS OF SOURCE SHAPE AND EVOLUTION IN TIME

We assume that the time derivative of stress glut tensor $\dot{\mathbf{\Gamma}}$ can be represented in the form:

$$\dot{\mathbf{\Gamma}} = f(\mathbf{x}, t)\mathbf{m} \tag{A1}$$

where $f(\mathbf{x}, t)$, the slip rate times μ, is a non-negative function.

Following Backus (1977a,b) we define the source region by the condition that the function $f(\mathbf{x}, t)$ is not identically zero and the source duration is the time during which inelastic motion occurs at various points within the source region, i.e. $f(\mathbf{x}, t)$ is different from zero. The spatial and temporal integral characteristics of the source can be expressed by the corresponding moments of the function $f(\mathbf{x}, t)$.

The spatio-temporal moments of $f(\mathbf{x}, t)$ of total degree 0, 1, and 2 with respect to point $\mathbf{q}$ and instant of time τ are defined as follows:

$$f^{(0,0)} = \int_V \mathrm{d}V \int_0^\infty f(\mathbf{x}, t)\,\mathrm{d}t \tag{A2}$$

$$f_i^{(1,0)}(\mathbf{q}) = \int_V \mathrm{d}V \int_0^\infty f(\mathbf{x}, t)\,(x_i - q_i)\,\mathrm{d}t \tag{A3}$$

$$f^{(0,1)}(\tau) = \int_V \mathrm{d}V \int_0^\infty f(\mathbf{x}, t)\,(t - \tau)\,\mathrm{d}t \tag{A4}$$

$$f_i^{(1,1)}(\mathbf{q}, \tau) = \int_V \mathrm{d}V \int_0^\infty f(\mathbf{x}, t)\,(x_i - q_i)\,(t - \tau)\,\mathrm{d}t \tag{A5}$$

$$f_{ij}^{(2,0)}(\mathbf{q}) = \int_V \mathrm{d}V \int_0^\infty f(\mathbf{x}, t)\,(x_i - q_i)\left(x_j - q_j\right)\,\mathrm{d}t \tag{A6}$$

$$f^{(0,2)}(\tau) = \int_V \mathrm{d}V \int_0^\infty f(\mathbf{x}, t)\,(t - \tau)^2\,\mathrm{d}t \tag{A7}$$

Using these moments the integral characteristics of the source are defined as follows. The source location is estimated by the spatial centroid $\mathbf{q_c}$ of the field $f(\mathbf{x}, t)$ as

$$\mathbf{q_c} = \mathbf{f}^{(1,0)}(\mathbf{0})/M_0 \tag{A8}$$

where $M_0 = f^{(0,0)}$ is the seismic moment.

The temporal centroid τ_c is

$$\tau_c = f^{(0,1)}(0)/M_0 \tag{A9}$$

The source duration Δt is estimated by $2\Delta\tau$ with

$$(\Delta\tau)^2 = f^{(0,2)}(\tau_c)/M_0 \tag{A10}$$

The spatial extend of the source is estimated by the matrix $\mathbf{W}$:

$$\mathbf{W} = \mathbf{f}^{(2,0)}(\mathbf{q}_c)/M_0 \tag{A11}$$

The mean source size in the direction $\mathbf{r}$ is estimated by the value $2l_r$ defined by the formula

$$l_r^2 = \mathbf{r}^T\mathbf{W}\mathbf{r} \tag{A12}$$

The source principal axes are directed along the eigenvectors of the matrix $\mathbf{W}$. The square of the length of the minor semi-axis is equal to the least eigenvalue, and the square of the length of the major semi-axis is equal to the greatest eigenvalue.

The average velocity $\mathbf{v}$ of the instant spatial centroid is estimated as

$$\mathbf{v} = \mathbf{w}/(\Delta\tau)^2, \tag{A13}$$

where

$$\mathbf{w} = \mathbf{f}^{(1,1)}(\mathbf{q}_c, \tau_c)/M_0. \tag{A14}$$